Published in final edited form as:

ACS Biomater Sci Eng. 2022 March 14; 8(3): 1239–1246. doi:10.1021/acsbiomaterials.1c01163.

Impact of membrane voltage on formation and stability of human renal proximal tubules *in vitro*

M. Adelfio[1,3], **M. Bonzanni**[1,4], **M. Levin**[2], **D.L. Kaplan**[1]

[1]Tufts University, Department of Biomedical Engineering, 4 Colby Street, Medford (02155), MA, USA.

[2]Tufts University, Biology Department, and Allen Discovery Center at Tufts University, 200 Boston Avenue, Medford (02155), MA, USA.

[3]Current affiliation: University of Massachusetts-Lowell, Department of Biomedical Engineering, 1 University Avenue, Lowell (01854), MA, USA.

[4]Current affiliation: Tufts University - School of Medicine, Department of Neuroscience, 136 Harrison Avenue Boston (02111), MA, USA.

Abstract

The membrane voltage (V_m) dynamics of a cell have been associated with cell migration, cell cycle progression, differentiation, and pattern formation. Kidney functions depend on the activity of ion channels, yet their role during tubulogenesis is unknown. Here we investigated the role of V_m during the *in vitro* tubulogenesis using human immortalized renal proximal tubule cells (RPTECs/TERT1). RPTECs were cultured on Matrigel to support the formation of proximal tubular-like structures with the incorporation of a voltage sensitive dye indicator – Bis-(1,3-Dibutylbarbituric Acid) Timethine Oxonol (DiBAC). The results demonstrated a correlation between the depolarization and the reorganization of human renal proximal tubule cells, indicating V_m as a candidate variable to control these events. Accordingly, V_m was pharmacologically manipulated using glibenclamide and pinacidil, K_{ATP} channel modulators, and then we reevaluated the impact on the V_m, proximal tubule formation and tubule stability over 21 days. Chronic manipulation of K_{ATP} channels induced changes in the tubular network topology without affecting lumen formation. Thus, a relationship was found between tubulogenesis and K_{ATP} channels. This relationship may provide future options as a control point during kidney tissue development, treatment, and regeneration goals.

Keywords

kidney; tubulogenesis; membrane potential; proximal; voltage

Corresponding Author: D. L. Kaplan, david.kaplan@tufts.edu.

Authors' contributions

M.A.: conceptualization, methodology, investigation, data curation, formal analysis, visualization, project administration, writing. **M.B.**: electrophysiology data collection. **M.L.**: funding acquisition, writing. **D.L.K.**: conceptualization, project administration, funding acquisition, writing. All authors read and approved the final manuscript.

Competing interests

The authors declare no competing financial interest.

Introduction

Many cell functions (i.e., migration, proliferation, differentiation, morphogenesis) can be regulated by bioelectric stimuli (1), which also help to orchestrate tissue- and organ-level events(2). Electrical events are characterized by a coordinated and directional movement of ions (i.e. Na^+, H^+, Ca^{2+}, K^+, Cl^-) across the cell membrane through ion channels; this ion flux generates a voltage difference between the inner and outer faces of the plasma membrane, known as voltage membrane potential (V_m). In the past, electrical events have been extensively studied in canonical excitable cells, such as neurons and cardiomyocytes, which can generate all-or-none events known as action potentials (3). However, non-excitable tissues also have a dynamic membrane potential, despite the absence of large fluctuations such as those seen with action potentials (4). The relationship between V_m and cellular physiology is reasonably conserved in different cell types (from precursor to mature cells, proliferative and quiescent cells, normal and cancerous cells), as well as between species (1). Endogenous bioelectric signaling events regulate cell migration, organ morphogenesis and size control through changes in V_m (5). This type of regulation can occur due to the complex apparatus (ion channels, pumps, transporters) present in a cell, which modulate electrical signals and coordinate cell behavior toward specific anatomical outcomes (1). The role of V_m in the formation and regulation of cell patterns has been modeled quantitatively(6, 7), as well as linked to biomechanical properties (8, 9); moreover, numerous mutations, which have been identified in genes encoding ion channels, were associated with defects in morphogenesis (10, 11).

All tissues, including the human kidney have a strong relationship between morphology and function. This correlation is particularly evident in the proximal segment of the renal nephron (12). Proximal tubules are characterized by a single layer of cuboidal polar epithelial cells, which self-assemble into tubular structures when grown on an appropriate extracellular matrix (13, 14). These cells also contain several ion channels and transporters, synchronized to regulate the processes of absorption and secretion in the proximal segment of the nephron (15). Electrophysiology studies on renal tissue have focused on physiological functions (15–17); however, the relationship between V_m and self-assembly of tubular structures has not been explored. Given the opportunity to develop new research tools to guide the formation of functional renal tubules in vitro for regenerative medicine purposes (18, 19), the goal of the present study was to investigate relationships between V_m and tubulogenesis. Using an *in vitro* 3D system to produce self-assembled functional tubules using human immortalized renal proximal tubule cells (hRPTEC/TERT1) embedded in Matrigel. The V_m trajectory was determined using a voltage sensitive dye, and subsequently, chronic modulation of potassium channels (K_{ATP}) was pursued by analyzing voltage and topological (tubular-like) profiles. The data showed that: 1) tubulogenesis trajectory was associated with overall depolarization of the structures, 2) K_{ATP} channel activity is important in defining tubular network topology, and 3) K_{ATP} channels can serve as intervention targets to modulate tubular formations *in vitro*. Overall, these data highlight a correlation between V_m and tubulogenesis in vitro and offer a path toward manipulating tubular network topology using bioelectrical cues.

Material and Methods

Cell culture

RPTEC/TERT1 (ATCC, Manassas, VA) were cultured in Dulbecco's Modified Eagle Medium/Nutrient Mixture F-12 (DMEM/F-12) (Thermo Fisher Scientific, Waltham, MA), containing L-glutamine and 4-(2-hydroxyethyl)-1-piperazineethanesulfonic acid (HEPES) and supplemented with 10 ng/mL of recombinant human Epidermal growth factor (EGF) (Thermo Fisher Scientific, Waltham, MA), 25 ng/mL prostaglandin E1 (Sigma-Aldrich, St. Louis, MO), 25 ng/mL hydrocortisone (Sigma-Aldrich, St. Louis, MO), 3.5 μg/mL L-ascorbic acid (Sigma-Aldrich, St. Louis, MO), 5 pM triiodo-L-thyronine (Sigma-Aldrich, St. Louis, MO), 1x Insulin-Transferrin-Selenium (ITS-G) (Thermo Fisher Scientific, Waltham, MA) and 100 μg/mL geneticin (Thermo Fisher Scientific, Waltham, MA). Cells were mycoplasma negative and were used up to 16 passages.

V_m trajectory and manipulation

RPTECs (1.32×10^5 cells/cm^2) were seeded onto black 24 well glass bottom plates (Cellvis, Mountain View, CA) coated with 300 μL of growth factor reduced Matrigel (Corning, NY) within a range of 7–8 mg/mL. Cells were left at 37 °C for 16 hours to induce the formation of an early network of proximal tubules and then covered with a second layer of Matrigel (285 μL) to obtain a 3D system (14). To manipulate the V_m, thirty minutes after seeding (day 0), the renal cells were chronically cultured with media supplemented with either Dimethyl Sulfoxide (DMSO) – *vehicle* (Sigma-Aldrich, St. Louis, MO), pinacidil 100 μM (Sigma-Aldrich, St. Louis, MO) or glibenclamide 50 μM (Sigma-Aldrich, St. Louis, MO). Cell cultures were analyzed at different days: 1,3,7,14,21.

Bis-(1,3-Dibutylbarbituric Acid) Timethine Oxonol- DiBAC

V_m values were analyzed by incubating proximal tubules with Bis-(1,3-Dibutylbarbituric Acid)Trimethine Oxonol) (DiBAC) (50 nM) (Thermo Fisher Scientific, Waltham, MA) in an extracellular-like solution (in mM: 75.4 NaCl, 70 mM KCl, $CaCl_2$ 1.8, $MgCl_2$ 1, Hepes NaOH 10, glucose 5.5, pH=7.4) until the stabilization of the signal (30–40 minutes), as per manufacturer instructions. The fluorescence signal was acquired at 37 °C with 5% CO_2 using a confocal microscope (Leica FLIM SP8); the acquisition settings were held constant among all experiments. For each sample, three images (after which the DiBAC signal usually starts to decrease) were acquired at 25X magnification. The images were exported as *.tif* files and analyzed with ImageJ as 8-bit files (NIH, Bethesda, MD). Fluorescence signal was quantified using z-stack maximum projections (20); the fluorescence background of the first image of the z-stack that was not in focus was used as a background reference point and subtracted from the maximum projection image. The DiBAC fluorescence intensity was quantified as Mean Grey Value in the selected proximal tubule structures. Proximal tubules structures were selected and analyzed using Region of Interest (ROI) manager settings in ImageJ; the images were zoomed in to visualize the cell boundaries within a tubule and the area that included the first and the last lane of cells in the tubular-like structures was chosen to define a proximal tubule (Supp. Figure 1). Maximum projection binary images were also exported as *.tif* files, imported into a custom MATLAB script and converted into heatmap images. To convert the fluorescence changes (ΔF) into

voltage changes (ΔV), the relation $\Delta V = \frac{\Delta F}{1.76}$ was used based on a previously published calibration curve (21), in which the relationship between DiBAC and voltage changes was assessed on RPTECs.

Electrophysiology

RPTECs (31,250 cells/cm^2) were cultured in 35-mm dishes (Corning, NY) coated with growth factor reduced Matrigel (Corning, NY) at 1 mg/mL. Patch clamp experiments in the whole cell configuration were conducted at room temperature while perfusing an extracellular solution containing (in mM): 75.4 NaCl, 70 mM KCl, $CaCl_2$ 1.8, $MgCl_2$ 1, Hepes NaOH 10, and glucose 5.5, pH=7.4. Borosilicate glass pipettes (7–9 MΩ) were filled with an ATP-free intracellular-like solution containing (in mM): 130 K-Gluc, 10 NaCl, 5 EGTA-KOH, 2 $MgCl_2$, 2 $CaCl_2$, 5 creatine phosphate, 0.1 GTP (Guanosine 5′-triphosphate sodium salt hydrate), and 10 Hepes-KOH, pH=7.2. The extracellular solution either contained DMSO (vehicle) or glibenclamide (50 μM; (22)). The native K_{ATP} current was evaluated with a ramp protocol (holding potential: −60 mV) of 400 ms duration between −120 mV and +40 mV as a glibenclamide-sensitive current. For each cell, the glibenclamide-sensitive current was computed by subtracting algebraically the current recorded in the presence of glibenclamide from the one recorded in DMSO. The reverse potential (E_{Rev}) was identified as the voltage at which the glibenclamide-sensitive current was zero. Liquid junctional potential was corrected as previously described (23).

Sholl Analysis and Tubule length

Sholl analysis was performed by imaging the whole well among the days (7 × 7 images) at 4X of magnification using an inverted microscope (Keyence BZ-X700) at different time points (day: 1,3,7,14 and 21). The images were then merged using the microscope associated software (Keyence, Elmwood Park, NJ). The number of intersections was analyzed by converting the images (.tif files) into binary images with ImageJ (NIH, Bethesda, MD) and were then normalized by the circumference of each circle used in the Sholl analysis (Suppl. Figure 2). The length of the tubules was analyzed by imaging three Regions of Interest (ROI) per condition at 4X magnification and using the ImageJ Simple Neurite Tracer (SNT) plugin. SNT was chosen because it considers the profile of the tubule instead of generating a straight line between two points. The tubules were defined as described above.

Immunohistochemistry

Lumen formation in proximal tubule structures (Suppl. Figure 4) was analyzed through immunohistochemistry. At day 21, cells were rinsed with phosphate buffered saline (PBS) 1x (Thermo Fisher Scientific, Waltham, MA), fixed in paraformaldehyde at 4% (Thermo Fisher Scientific, Waltham, MA) in PBS for 30 minutes and permeabilized with Triton X (Sigma-Aldrich, St. Louis, MO) 0.5% in PBS for 30 minutes. Cells were blocked with Bovine Serum Albumin (BSA) 1% (Sigma-Aldrich, St. Louis, MO) in PBS for one hour and then incubated with 4′,6-diamidino-2-phenylindole (DAPI) in PBS 1x (Thermo Fisher Scientific, Waltham, MA) for 20 minutes.

Results

Membrane voltage depolarization during tubulogenesis

To assess a potential association between structural changes during *in vitro* tubulogenesis and cell membrane voltage (V_m), the V_m was measured using a fluorescent dye (DiBAC). In Fig.1A, representative heatmap image shows increased intensity of the DiBAC signal over time, indicative of depolarization of V_m compared to day 1. In Fig.1B (top), the percentage of Mean Fluorescence Intensities (MFI) normalized on day 1 are shown over time, indicating the increase of DiBAC intensity started at day 3 and plateaued after day 7 (% of Norm. MFI: day 3: 140.6±2.2, n=4; day 7: 210.7±3.8, n=4; day 14: 219.1±9.2, n=5; day 21: 195.4±6.9, n=3). Using a calibration curve previously described (21), the DiBAC intensity changes were converted into ΔV values (V_m difference between the indicated day and day 1). Compared to day 1, at day 3 the V_m depolarization was +7.2±2.6 mV, +17.6±3.4 mV at day7, +19.0±3.8 mV at day 14 and +11.8±3.5 at day 21 (Fig.1B, bottom). Overall, the results indicated that depolarization occurred during tubulogenesis, which stabilized at day 7 and was then maintained through day 21.

In view of the role of K_{ATP} channels during cell migration and proliferation (24), and since these channels were already associated with the formation of *in vitro* rat collecting-duct tubules (25), we hypothesized that these channels could play a role in tubulogenesis. First, the presence of K_{ATP} current (I_{KATP}) was confirmed using patch clamp (n. cells=7). The native current was assessed as a glibenclamide-sensitive current using a ramp voltage protocol (Fig.1C, top) with cells bathed with an extracellular solution containing $[K^+]_{out}$=70 mM and dialyzed in an ATP-free solution. In Fig.1C (bottom), representative current traces are shown applying the indicated voltage protocol (blue trace); after switching the external solution from vehicle (DMSO) to glibenclamide (green and red traces, respectively), the current decreased in response to the closure of the K_{ATP} channels (the resulting glibenclamide-sensitive current is shown in black as the algebraical difference between the DMSO and glibenclamide traces). The current reduction applying glibenclamide was then quantified at the holding potential (h.p.=−60 mV); the decreased current ($p<0.005$) is shown in Fig.1D (left; in pA: DMSO: −221.5±10.8; Glibenclamide: −196.5±11.2), indicating the presence of the K_{ATP}-mediated current. The density current-voltage plot (Fig.1 E) was then reconstructed as glibenclamide-sensitive (black trace) confirming the presence of the K_{ATP} current in the RPTECs. The reverse potential (E_{Rev}) was then identified for each cell (Fig.1D, right: −13.8±3.14 mV): the value agreed ($p=0.28$, One-Sample T-Test) with the Nernst potential for potassium for the used solutions (−17.5 mV at T=293.15K), confirming the permeability to potassium of the blocked channels. Overall, the functional expression of the K_{ATP} conductance in the RPTECs was confirmed.

Membrane voltage was unaffected by chronic K_{ATP} modulation during tubulogenesis

After functional confirmation of the presence of I_{KATP} in the RPTEC cells, we chronically manipulated the channel activity by either using a channel opener (pinacidil) or blocker (glibenclamide), with the initial aim of evaluating the role of K_{ATP} channels along the V_m trajectory. The V_m was once again quantified using DiBAC; in Fig.2A, representative heatmap images are shown in the different conditions and days, as indicated. The V_m

readings were variable in all conditions, as evident in Fig.2B (left), where the DiBAC intensities for all the conditions (DMSO: black; pinacidil: orange; glibenclamide: green) are shown at each day. The logarithm of the DiBAC intensity ratios at each day and condition is then shown in Fig.2B (right) for pinacidil and glibenclamide (left and right, respectively) over time, each normalized on their day-matched DMSO condition; since the ratios are shown as logarithms, negative values indicate hyperpolarization of the V_m (light yellow: ratio smaller than 1, lower DiBAC signal in the condition *vs* day-matched DMSO), while positive values indicate depolarization of the V_m (light pink: ratio higher than 1, higher DiBAC signal in the condition *vs* day-matched DMSO) compared to the DMSO condition. The day-matched comparisons between pinacidil *vs* glibenclamide did not show any significant differences over time. Overall, the chronic treatments did not impact the V_m during tubulogenesis, at least based on the current methodology (DiBAC) and conditions utilized in these experiments.

Chronic K_{ATP} modulation affected tubular topology

Since ions can act as second messengers and ion channels can transduce signals beyond changes in V_m, we then evaluated the impact of chronic activation (pinacidil) or blocking (glibenclamide) the K_{ATP} channels on tubular topology. In Fig. 3A, representative image insets of tubular formation are shown for the different conditions (row-wise) and at different days (column-wise), suggesting a treatment-specific phenotype; for each condition, the evolution of morphology over time of the same well is shown. First, we quantified the number of intersections using Sholl analysis, with circles of increasing radius from center to edge (Supplementary Fig. 2). For each circle, we computed the number of intersections and normalized them with the value of the circumference ($2\pi r$; 0 indicating the center of the dish in the scale bar of Fig. 3A), obtaining the number of intersections per unit of space (mm). Since the number of normalized intersections near the center was not statistically different from that near the edge under all conditions (Fig. 3B), it was evident that the tubular formations were uniformly distributed in the dish, and this behavior was not altered by the treatments. We then averaged the number of intersections/mm over the entire surface of the dish (Fig. 3C). We found that the intersections/mm in the presence of the pinacidil (opener) were statistically higher than those of both DMSO and glibenclamide at every day, where the glibenclamide (blocker) condition had more intersections/mm ($p<0.05$) than DMSO only at day 1. Moreover, it is important to note that the number of intersections decreased until day 7 for all conditions, and then stabilized; such decrease was more pronounced for the DMSO and glibenclamide conditions than for pinacidil (Supplementary Figure 3, left; Supplementary Table 1). We finally quantified the tubule length (Fig.3D) and found that the pinacidil condition had shorter tubules compared to both DMSO and glibenclamide ($p<0.05$), while glibenclamide had shorter tubules than DMSO at all days but day 21 and longer tubules than pinacidil at all time points. For all the conditions, the tubule length increased until day 7, reached a plateau until day 14 and finally decayed at day 21 (Supplementary Figure 3, right; Supplementary Table 1). In all conditions, at day 21, the lumen cavity was properly formed (Supplementary Figure 4). Overall, the chronic opening (pinacidil) of the K_{ATP} channels led to a denser tubular structure (more intersections/mm and less pronounced decay over time) with shorter tubules compared to the DMSO condition; the chronic blockage (glibenclamide) of the K_{ATP} channels did not affect the density of the

tubular structures but led to shorter and truncated tubules compared to the DMSO condition (also evident from the representative structures in Fig.2A).

Discussion

Variations in membrane voltage (V_m) resulting from the movement of ions across the membrane have been associated with many physiologically-relevant tasks beyond the generation of action potentials, such as proliferation, differentiation, migration, and apoptosis (26). In addition, point mutations in genes encoding ion channels can lead to diseases associated with morphological rather than electrical malfunctions, such as the Andersen-Tawil syndrome, cardiac morphology defects and tracheal morphogenesis (26–28). In fact, one of the most intriguing processes associated with bioelectric signals is the definition of the shape and morphology of organs. Both V_m and ion channel functions have been associated with migration, cell motility, shape and pattern specification spanning the entire phylogenetic tree, from zebrafish to humans (10); all these events are crucial in defining the proper morphology of a tissue, an organ, and a body (29). The importance of bioelectrical clues is also highlighted by its effectiveness in guiding tissue regeneration (30–32).

One of the most challenging, diverse, and widespread structures in living organisms is represented by tubules, which can be defined as sheets of cells enclosing an empty lumen (29). Despite its simple definition, the tubulogenesis process involves the orchestrated activity of multiple molecular pathways (i.e., cell surface receptors, cell matrix, adhesion molecules) and physical forces (29). Among tubular organs, the kidney is one of the most studied; considering the incidence of renal diseases (33), which usually is accompanied by the need for a transplant, the development of strategies to either enhance renal repair and/or generate new bioengineered nephrons (34). In view of the role of V_m in shaping organ morphologies (9), and the need to find strategies to produce new tubular units for translational/regenerative medicine purposes, we hypothesized that bioelectric events could be involved in tubulogenesis and could serve as modulators of this process.

In the present study we explored the potential association between V_m, K_{ATP} channels and the generation of *in vitro* renal tubular structures. We first assessed changes of the V_m during tubulogenesis. We utilized DiBAC, a voltage sensitive dye, as it had two important advantages over the patch clamp approach in the current experimental design: the dye preserved the integrity of the intracellular environment of the cells, and the approach allowed the recording of the entire 3D sample. We found that over time, the V_m of the tubular network depolarized (higher DiBAC intensity), indicating a correlation between the morphological changes and the V_m (Fig.1A,B). In particular, the depolarization occurred between days 1 and 7, after which it stabilized. It is known that these cells start to self-assemble after 3–5 days in culture, with the formation of a major lumen around day 10 (35); in addition, it is known that renal cells are highly polarized and surrounded by a well-defined lumen around day 23, as previously described (14). We can therefore hypothesize that V_m was mainly involved and/or modified in response to the self-assembly phase of the cells, rather than in the formation of the lumen cavity. Renal tubules are formed by budding, which is the process of invagination of a sheet of polarized cells or the formation of new

branches in a pre-existing tubule (36). Before the expansion of the luminal space, cell-cell and cell-matrix interactions must be established, which are followed by the generation of an apical-basal polarity and shape changes and movements of the cells (36). In the present work, we have not explored, nor do we claim, any causal relationship between the V_m and the pre-luminal phase events. On the basis of our data, we can only highlight the similarities of the temporal profiles of the V_m trajectory (Fig.1B), the number and length of tubules (Supplementary Figure 3), speculating on a correlation between the trajectory of V_m and the phase preceding the luminal space expansion. Indeed, it appears that the changes in all parameters occurred before day 7 (pre-luminal phase), after which a rather stable plateau from both the voltage and morphological perspective was reached.

We then explored if the modulation of a single ion channel, K_{ATP}, could be involved in the process and, potentially, could serve as a morphogen modulator. The main advantage of focusing on a single target is the specificity of manipulation; the activity of single channels can be controlled using specific drugs without affecting the composition of the environment, differently from broader yet less specific manipulations (such as the change of the ionic composition of the extracellular solution). The reason to focus on K_{ATP} channels as a target was grounded in the literature (24, 25, 37, 38), but it is also quite arbitrary; indeed, since so little is known about the involvement of ion channels in the tubulogenesis process, there is no privileged target from which to start. K_{ATP} channels have been previously associated with the development of the rat collecting-duct epithelium (25); where they showed that the K_{ATP} channels were involved in the early events leading to the generation of the ureteric bud. Moreover, they showed that pinacidil, a K_{ATP} opener, was able to increase the *in vitro* tubulogenesis of the collecting duct. In our model, after confirming the functional expression of the K_{ATP} channels using a patch clamp approach (Fig.1C–E), we found that the chronic block (using glibenclamide) or chronic activation (pinacidil) did not induce a change of V_m (Fig.2) when compared with the chronic vehicle treatment (DMSO). It is important to note that the V_m trajectory in DMSO (Fig.2B) did not resemble that of the extracellular-like solution (Fig.1B): indeed, even though a depolarization was evident between days 1 and 3 in DMSO, such depolarization was not maintained throughout the entire trajectory. The absence of any change of V_m must be considered in view of the difficulty to capture either transient events or small fluctuations with the current methodology. In fact, it is likely that, if K_{ATP} could actually impact the V_m, such modulation could be transient, and may have missed the time window in our present analysis. In addition, the K_{ATP} conductance may be small and therefore have minimal impact on the V_m, and that change may have been below the DiBAC detection limit; a similar scenario is also possible with an overall low input resistance.

On the other hand, ion channels are also known to transduce signals beyond the V_m. In this view, the lack of any detectable V_m changes is not a sufficient reason to exclude a role of K_{ATP} channels in the tubulogenesis process. Indeed, we found that the chronic treatments did impact the topology of tube formation (Fig.3). The chronic activation of the K_{ATP} channels led to denser tube formation; such higher density was accompanied by a shorter length of each tubule. These results are in line with those of Braun and colleagues obtained in the rat collecting duct (25); the similar effect on two different cells and lineages could suggest a more general role of K_{ATP} in tubule formation. The chronic block of K_{ATP},

in contrast, only resulted in shorter and truncated tubules, which are also more prone to die and detach. In all treatments, the lumen was properly formed (Supplementary Figure 4), reinforcing the hypothesis that the pre-luminal phases, but not lumen formation, were influenced by K_{ATP} modulators. Overall, K_{ATP} channels influenced tubulogenesis; if this action is exploited or not by changes in V_m, cannot be ruled out based on the data collected in the present work.

The use of DiBAC, even if advantageous as reported here, has several limitations to be considered, including: 1) the background noise of the 3D system decreases the probability of recording small fluctuations in V_m; 2) we cannot record the same sample for an extended period of time, impinging our ability to detect transient changes of voltage and to evaluate the evolution of the same sample over time. For each sample, moreover, we did not perform an analysis of the DiBAC at single cell resolution, but rather we analyzed the average DiBAC intensity of the structures; a single cell analysis could, on the other hand, reveal spatial information that we have not considered in the present study. To overcome these technical limitations, future experiments should be performed by generating stable cell lines that overexpress genetically encoded voltage indicators (GEVIs; (39)). Due to methodological issues, we did confirm the functional expression of K_{ATP} channels in a 2D culture rather than in the 3D model. From a cellular perspective, even though RPTECs are human cells, Matrigel is derived from murine sarcoma, thus preventing any potential implantation of the current model beyond a murine model.

Conclusions

We showed a correlation between V_m and tubulogenesis exists *in vitro* and that the topology of the resulting tubular structures can be modulated via K_{ATP} channels. In consideration of the low rate of effective implant of bioengineered renal devices, the probability of successful functional engraftment could benefit from a denser tubular structure, like those obtained using pinacidil. Such results offer a potential path forward in new options to modulate cells and tissues in conjunction with regenerative options for kidney tissues.

Supplementary Material

Refer to Web version on PubMed Central for supplementary material.

Acknowledgements

The authors thank Joshua Erndt-Marino for his technical assistance.

Funding

We thank the NIH (R24DK106743; P41EB027062) and the Paul Allen Foundation (2171) for funding and the inputs from the Re-Building a Kidney consortium.

Availability of data and materials

All data generated or analyzed during this study are included in this published article.

List of abbreviations

DIBAC	Bis-(1,3-Dibutylbarbituric Acid) Timethine Oxonol
RPTECs/TERT1	human immortalized renal proximal tubule cells
V_m	membrane potential

References

1. Levin M, Pezzulo G, Finkelstein JM. Endogenous Bioelectric Signaling Networks: Exploiting Voltage Gradients for Control of Growth and Form. Annu Rev Biomed Eng. 2017;19:353–87. [PubMed: 28633567]
2. Levin M Bioelectric signaling: Reprogrammable circuits underlying embryogenesis, regeneration, and cancer. Cell. 2021.
3. Hille B Ion channels of excitable membranes. 3rd ed. Sunderland, Mass.: Sinauer; 2001. xviii, 814
4. Abdul Kadir L, Stacey M, Barrett-Jolley R. Emerging Roles of the Membrane Potential: Action Beyond the Action Potential. Front Physiol. 2018;9:1661. [PubMed: 30519193]
5. A Meta-Analysis of Bioelectric Data in Cancer, Embryogenesis, and Regeneration.0(0):null.
6. Pietak A, Levin M. Bioelectric gene and reaction networks: computational modelling of genetic, biochemical and bioelectrical dynamics in pattern regulation. J R Soc Interface. 2017;14(134).
7. Cervera J, Pai VP, Levin M, Mafe S. From non-excitable single-cell to multicellular bioelectrical states supported by ion channels and gap junction proteins: Electrical potentials as distributed controllers. Progress in biophysics and molecular biology. 2019;149:39–53. [PubMed: 31255702]
8. Leronni A, Bardella L, Dorfmann L, Pietak A, Levin M. On the coupling of mechanics with bioelectricity and its role in morphogenesis. J R Soc Interface. 2020;17(167):20200177. [PubMed: 32486953]
9. Silver BB, Wolf AE, Lee J, Pang MF, Nelson CM. Epithelial tissue geometry directs emergence of bioelectric field and pattern of proliferation. Molecular biology of the cell. 2020;31(16):1691–702. [PubMed: 32520653]
10. Whited JL, Levin M. Bioelectrical controls of morphogenesis: from ancient mechanisms of cell coordination to biomedical opportunities. Curr Opin Genet Dev. 2019;57:61–9. [PubMed: 31442749]
11. Lanni JS, Peal D, Ekstrom L, Chen H, Stanclift C, Bowen ME, et al. Integrated K+ channel and K+Cl- cotransporter functions are required for the coordination of size and proportion during development. Dev Biol. 2019;456(2):164–78. [PubMed: 31472116]
12. Welling LW, Welling DJ. Relationship between structure and function in renal proximal tubule. 1988;9(2):171–85.
13. Adelfio M, Szymkowiak S, Kaplan DL. Matrigel-Free Laminin–Entactin Matrix to Induce Human Renal Proximal Tubule Structure Formation In Vitro. ACS Biomaterials Science & Engineering. 2020;6(12):6618–25. [PubMed: 33320630]
14. Secker PF, Luks L, Schlichenmaier N, Dietrich DR. RPTEC/TERT1 cells form highly differentiated tubules when cultured in a 3D matrix. Altex. 2018;35(2):223–34. [PubMed: 29197217]
15. Kuo IY, Ehrlich BE. Ion channels in renal disease. Chem Rev. 2012;112(12):6353–72. [PubMed: 22809040]
16. Blackburn JG, Hazen-Martin DJ, Detrisac CJ, Sens DA. Electrophysiology and ultrastructure of cultured human proximal tubule cells. Kidney Int. 1988;33(2):508–16. [PubMed: 3361752]
17. Sackin H, Palmer LG. Basolateral potassium channels in renal proximal tubule. Am J Physiol. 1987;253(3 Pt 2):F476–87. [PubMed: 2443019]
18. Bhavsar MB, Leppik L, Costa Oliveira KM, Barker JH. Role of Bioelectricity During Cell Proliferation in Different Cell Types. Front Bioeng Biotechnol. 2020;8:603. [PubMed: 32714900]

19. Blackiston DJ, McLaughlin KA, Levin M. Bioelectric controls of cell proliferation: ion channels, membrane voltage and the cell cycle. Cell Cycle. 2009;8(21):3527–36. [PubMed: 19823012]
20. Adams DS, Masi A, Levin M. H^+ pump-dependent changes in membrane voltage are an early mechanism necessary and sufficient to induce *Xenopus* tail regeneration. Development. 2007;134(7):1323. [PubMed: 17329365]
21. Bonzanni M, Payne SL, Adelfio M, Kaplan DL, Levin M, Oudin MJ. Defined extracellular ionic solutions to study and manipulate the cellular resting membrane potential. Biol Open. 2020;9(1).
22. Engbersen R, Masereeuw R, van Gestel MA, van der Logt EM, Smits P, Russel FG. Glibenclamide depletes ATP in renal proximal tubular cells by interfering with mitochondrial metabolism. Br J Pharmacol. 2005;145(8):1069–75. [PubMed: 15912128]
23. Neher E Correction for liquid junction potentials in patch clamp experiments. Methods Enzymol. 1992;207:123–31. [PubMed: 1528115]
24. Girault A, Brochiero E. Evidence of K+ channel function in epithelial cell migration, proliferation, and repair. Am J Physiol Cell Physiol. 2014;306(4):C307–19. [PubMed: 24196531]
25. Braun GS, Veh RW, Segerer S, Horster MF, Huber SM. Developmental expression and functional significance of Kir channel subunits in ureteric bud and nephron epithelia. Pflügers Archiv. 2002;445(3):321–30. [PubMed: 12466933]
26. Levin M, Stevenson CG. Regulation of cell behavior and tissue patterning by bioelectrical signals: challenges and opportunities for biomedical engineering. Annu Rev Biomed Eng. 2012;14:295–323. [PubMed: 22809139]
27. Masotti A, Uva P, Davis-Keppen L, Basel-Vanagaite L, Cohen L, Pisaneschi E, et al. Keppen-Lubinsky syndrome is caused by mutations in the inwardly rectifying K+ channel encoded by KCNJ6. American journal of human genetics. 2015;96(2):295–300. [PubMed: 25620207]
28. Kortüm F, Caputo V, Bauer CK, Stella L, Ciolfi A, Alawi M, et al. Mutations in KCNH1 and ATP6V1B2 cause Zimmermann-Laband syndrome. Nature genetics. 2015;47(6):661–7. [PubMed: 25915598]
29. Iruela-Arispe ML, Beitel GJ. Tubulogenesis. Development. 2013;140(14):2851–5. [PubMed: 23821032]
30. McLaughlin KA, Levin M. Bioelectric signaling in regeneration: Mechanisms of ionic controls of growth and form. Dev Biol. 2018;433(2):177–89. [PubMed: 29291972]
31. Busse SM, McMillen PT, Levin M. Cross-limb communication during Xenopus hindlimb regenerative response: non-local bioelectric injury signals. Development. 2018;145(19).
32. Sousounis K, Erdogan B, Levin M, Whited JL. Precise control of ion channel and gap junction expression is required for patterning of the regenerating axolotl limb. Int J Dev Biol. 2020;64(10-11-12):485–94. [PubMed: 33200809]
33. Luyckx VA, Al-Aly Z, Bello AK, Bellorin-Font E, Carlini RG, Fabian J, et al. Sustainable Development Goals relevant to kidney health: an update on progress. Nat Rev Nephrol. 2021;17(1):15–32. [PubMed: 33188362]
34. Schold JD, Segev DL. Increasing the pool of deceased donor organs for kidney transplantation. Nat Rev Nephrol. 2012;8(6):325–31. [PubMed: 22450438]
35. Schumacher KM, Phua SC, Schumacher A, Ying JY. Controlled formation of biological tubule systems in extracellular matrix gels in vitro. Kidney Int. 2008;73(10):1187–92. [PubMed: 18288104]
36. Marciano DK. A holey pursuit: lumen formation in the developing kidney. Pediatr Nephrol. 2017;32(1):7–20. [PubMed: 26902755]
37. Quast U ATP-sensitive K+ channels in the kidney. Naunyn Schmiedebergs Arch Pharmacol. 1996;354(3):213–25. [PubMed: 8878050]
38. Mauerer UR, Boulpaep EL, Segal AS. Regulation of an inwardly rectifying ATP-sensitive K+ channel in the basolateral membrane of renal proximal tubule. J Gen Physiol. 1998;111(1):161–80. [PubMed: 9417142]
39. Mollinedo-Gajate I, Song C, Knopfel T. Genetically Encoded Voltage Indicators. Adv Exp Med Biol. 2021;1293:209–24. [PubMed: 33398815]

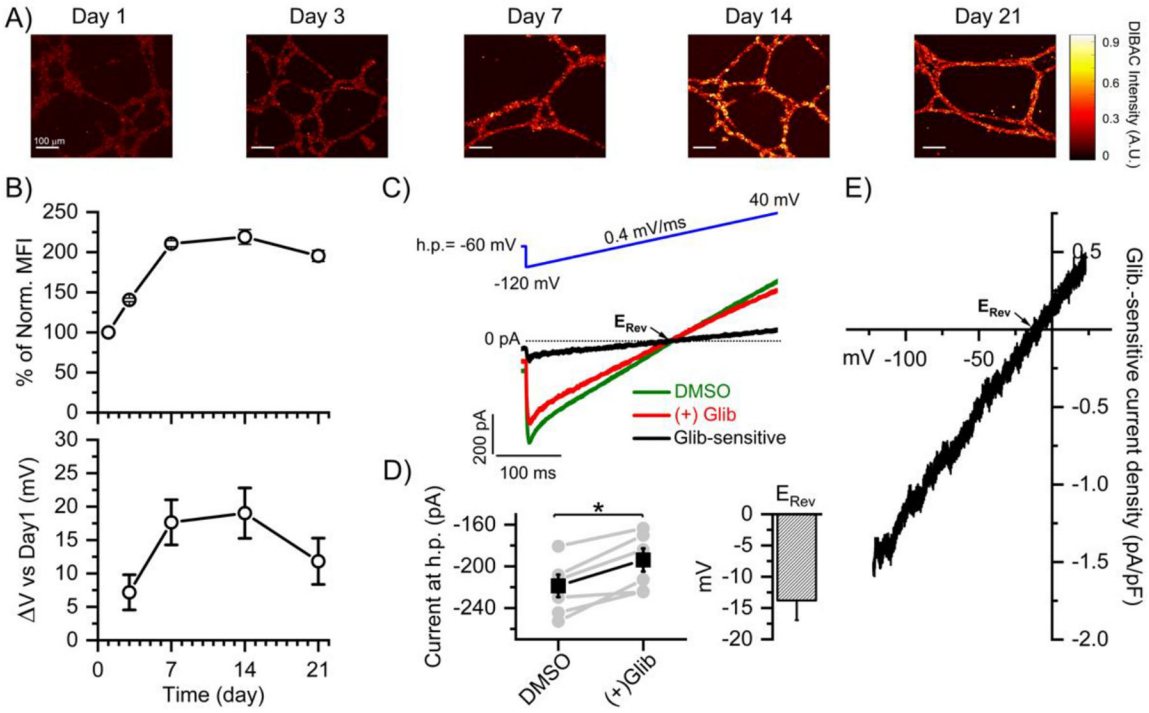

Figure 1. V_m trajectory during cell reorganization and K_{ATP} electrophysiological properties in RPTECs.

A) Representative heatmap images of normalized DiBAC signal. Scale bar: 100 μm. **B)** Percentage of MFI intensity trajectory normalized on day 1 (top) and ΔV voltage trajectory compared to day 1 (bottom). **C)** Voltage protocol (top, blue; holding potential (hp)=−60 mV, from −120 mV to 40 mV, 400 ms duration) and representative current traces (bottom) in DMSO (green) and glibenclamide (red) conditions; the glibenclamide-sensitive current trace is shown in black. **D)** The amount of I_{KATP} current at the holding potential before and after application of glibenclamide in the bath (grey circles); mean I_{KATP} currents at the holding potential in DMSO and glibenclamide (black squares). On the right, the mean E_{Rev} identified as the voltage at which the current flow was zero (indicated with an arrow in panel E). **E)** Mean glibenclamide-sensitive current density-voltage plot. *p=0.005. Paired T-Students test. Data shown as Mean ± S.E.M.

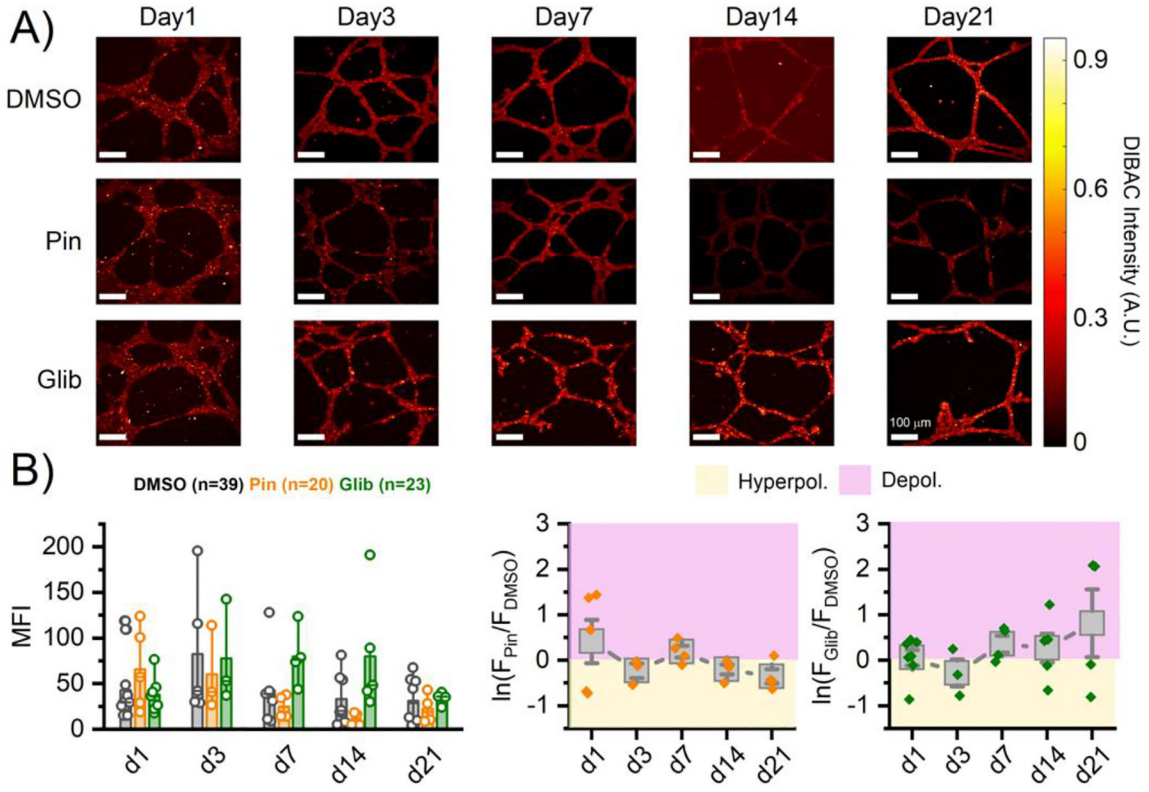

Figure 2. The V_m trajectory was not affected by chronic manipulation of the K_{ATP} channels.

A) Representative heatmap images of normalized DiBAC signal for the different conditions and days, as indicated. Scale bar: 100 µm. **B)** Single MFI values (circles) and mean MFI intensities (bar graphs) for DMSO, pinacidil and glibenclamide (black, orange, and green, respectively). Single logarithmic ratios (pinacidil/DMSO and glibenclamide/DMSO; diamonds) and mean logarithmic ratios (box plots) for the two treatments. Number of experiments per day: day 1 DMSO (8), pinacidil (5) and glibenclamide (7); day 3 DMSO (6), pinacidil (3) and glibenclamide (3); day 7 DMSO (8), pinacidil (4) and glibenclamide (4); day 14 DMSO (8), pinacidil (4) and glibenclamide (5); day 21 DMSO (7), pinacidil (4) and glibenclamide (4).

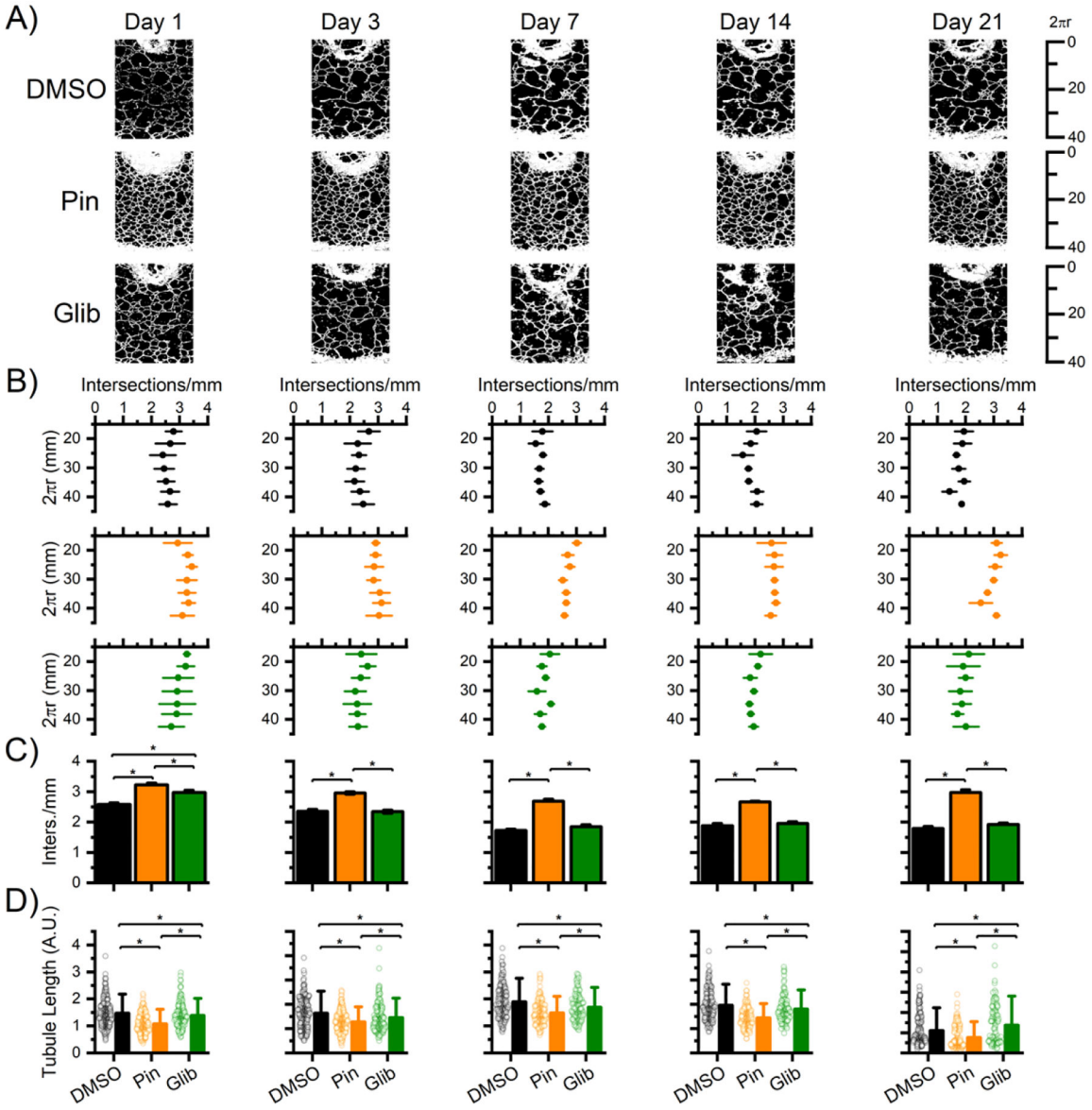

Figure 3. The K_{ATP} channels shape density and length of tubular structures.

A) Representative tubular formation for the different conditions and days, as indicated. **B)** Number of intersections/mm (x-axis) as a function of the circumference values (y-axis) of the circles used for the Sholl analysis. **C)** Mean intersections/mm and **D)** tubule lengths for the different conditions and days, as indicated. *p<0.05, One-Way ANOVA, Fisher post-hoc test. Number of experiment 3 and number of tubules analyzed 66/3 images.